Properties of the solid-liquid interface of growing salol crystals: A dynamic light scattering investigation

U. Dürig, J. H. Bilgram, and W. Känzig
Laboratory of Solid State Physics, Swiss Federal Institute of Technology, CH-8093 Zürich, Switzerland
(Received 21 February 1984)

The freezing process has been studied by means of quasielastic light scattering at the solid-liquid interface of growing salol crystals. In the range of the investigated growth velocities, 0.2 μm/s $\leq v_k \leq$ 0.8 μm/s, we observe two different dynamical processes at the interface, which can be distinguished by the scattered light. In a first process intense Rayleigh scattering sets in if a critical growth velocity is exceeded, which for growth along the [010] axis is in the range of 0.2 μm/s $\leq v_{crit} \leq$ 0.8 μm/s. Intensity measurements suggest that the scattering arises from fluctuations in an interface layer of a thickness of the order of 1 μm. The spectrum of the scattered light can be fitted by a single Lorenzian with a linewidth $\Gamma = D_i q^2$ ($\vec{q}$ is the scattering vector). The thus obtained value of the diffusion constant, $D_i = (1.0 \pm 0.25) \times 10^{-9}$ cm^{2}s^{-1}, is by 6 orders of magnitude smaller than the thermal diffusivity of liquid salol. In a second process the light is scattered by a propagating line-grating-like structure, which we interpret in terms of almost equidistant steps of growth spirals originating at screw dislocations. The step spacing d was determined from the angular distribution of the scattered intensity, and the step velocity v_s from the Doppler shift. For a growth velocity $v_k = 0.5$ μm/s perpendicular to the (001) facet typical values are $d = 0.4$ μm and $v_s = 40$ μm/s. For the step height $h = v_k d / v_s$ we obtain values of the order of 2.5 lattice constants. The product $v_s d$ is independent of v_k and has a value of $(1.8 \pm 0.4) \times 10^{-7}$ cm^{2}s^{-1}, whereas v_s is proportional to the square root of v_k. An interpretation of the data is presented.

I. INTRODUCTION

The dynamics of crystal growth from the melt are determined by two processes: the diffusion of latent heat and the ordering of molecules. For example, in theory of dendritic growth[1] the interaction of the temperature field with the processes occurring at the advancing crystal front is crucial. However, at the comparatively low rates at which large single crystals grow the growth kinetics are dominated by the lattice formation. This process is little understood because the solid-liquid interface is not in thermodynamic equilibrium.

In the well-known phenomenological theories of crystal growth due to the Wilson,[2] Frenkel,[3] Becker and Döring,[4] and Burton, Cabrera, and Frank[5] a sharp phase boundary is assumed. Molecular dynamics simulations of crystal growth from the melt at nonequilibrium conditions (Landman *et al.*[6]) yield a stratified interface layer with a thickness of about five lattice spacings.

Light scattering experiments at the solid-liquid interface of growing ice crystals[7] have shown that a dynamical structure giving rise to intense light scattering builds up at the interface if a critical growth velocity is exceeded. Subsequent experiments[8] have shown that the light scattering arises from density fluctuations in an interface layer of a few μm thickness. These fluctuations decay about 5 orders of magnitude slower than density fluctuations in bulk water. In order to check whether the observed phenomenon is an anomaly of the ice-water system we performed similar experiments on salol crystals. Already the early experiments revealed[9] that, in addition to diffusively decaying inhomogeneities, propagating structures are present at the solid-liquid interface. Cummins and co-workers[10] recently reported on results of their light scattering experiments at the phase boundary of salol. Their results agree in most points with ours. The propagating structure was interpreted in terms of growth steps originating from screw dislocations.

The present work is a detailed account of our light scattering experiments. We find that the propagating structure scatters like an imperfect moving line grating. We were able to measure *in situ* simultaneously the propagation velocity and the grating period. Interpreting this structure as growth spirals emanating from screw dislocations we have compared our results with calculations based on ideas developed in Ref. 5. We also measured intensity and linewidth of the light scattered by the diffusive fluctuations. The results support the view that the scattered light originates from an interface layer of a thickness of at least 1 μm in which density fluctuations decay at a rate which is by 6 orders of magnitude smaller than in the bulk liquid. A tentative interpretation of this slow decay is given inspired by the theory of critical phenomena.

II. THE SUBSTANCE

A. Crystal preparation

Light scattering experiments at the solid-liquid interface are done *in situ* on crystals growing in a zone-refining apparatus (Fig. 1). The salol single crystals (the structure is shown in Fig. 2) used in the experiment are enclosed in an evacuated zone-refining tube of 15 mm

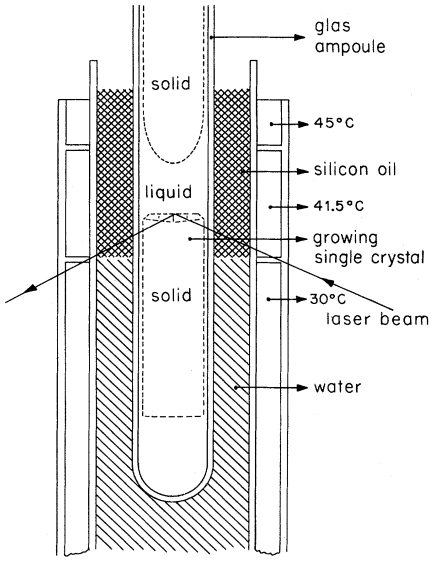

FIG. 1. Zone melting apparatus.

inner diameter. The length of the crystal is about 150 mm. Two types of samples were prepared, one with the [001] axis and one with the [010] axis parallel to the cylinder axis. Frequent zone refining of the crystals is necessary to assure a good quality of the solid-liquid interface. It has been found that an interval of more than two months between two successive zone-refining passes of a given crystal results in an increase of the concentration of inhomogeneities at the solid-liquid interface that are detectable by light scattering. On the other hand, we observed an increasing tendency for strain cracks to appear in the crystals with each zone-refining pass. Details about the sample preparation and the crystal structure are described in Ref. 11.

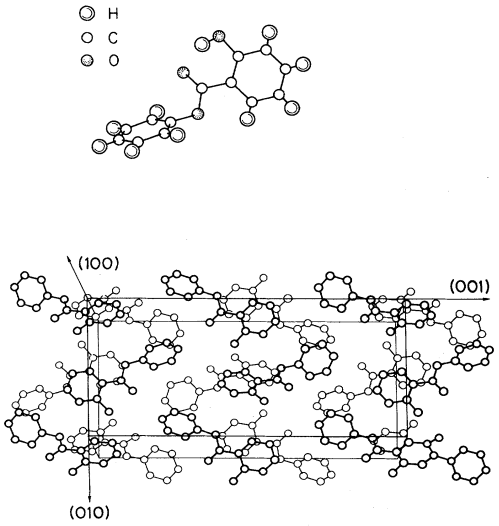

FIG. 2. Molecular and crystalline structure of salol. The dimensions of the unit cell are (20°C) 8.0 Å [100], 11.3 Å [010], 23.8 Å [001].

TABLE I. Refractive index of liquid salol ($20°C \leq T \leq 50°C$, λ is the wavelength of the light). $n(T)=n_0+\alpha T$.

λ (nm)	n_0	α ($°C^{-1}$)
488	1.6167	−0.000 46
514.5	1.6104	−0.000 45
632.8	1.5926	−0.000 43

B. Optical properties

Crystalline salol is strongly birefringent. The refractive indices of the crystalline and the liquid salol are such that a light beam appropriately polarized coming from the solid or the liquid side can be totally reflected at the phase boundary. We have measured by means of a temperature-controlled Abbé refractometer (Zeiss) the refractive index of liquid salol. In the temperature range $20°C \leq T \leq 50°C$ the measured values can be fitted with a relative error of 10^{-4} by

$$n(\lambda,T)=n_0(\lambda)+\alpha(\lambda)T \ . \tag{2.1}$$

The values of n_0 and α for different wavelengths of the light are listed in Table I. The principal refractive indices of the crystal are[10] ($\lambda=488$ nm) $n_{[001]}=1.552$, $n_{[010]}=1.663$, $n_{[001]}=1.827$ (see Fig. 2 for the nomenclature of the axes).

III. EXPERIMENTAL SETUP

The ampoule containing the crystal under investigation is lowered into the cooling bath of the zone-refining apparatus at a constant velocity v_k (Fig. 1). A steady state develops in which the growth velocity of the crystal is equal to v_k, the position of the solid-liquid interface being at rest in the laboratory system.

The interface is illuminated from the crystal side by a laser beam. We use an argon laser (Spectra Physics Model 165) at 488 nm and a krypton laser (Spectra Physics Model 171) at 647.1 nm simultaneously (Fig. 3). The two beams merge in a beam splitting cube. They then pass through the same spatial filter ($L1, A1$) and expansion lens ($L2$, achromat $f=30$ mm). By these means the two beams are made perfectly collinear. Radiation of either wavelength is selected by opening a shutter in front of the appropriate laser. The light focused by the lens $L3$ ($f=500$ nm) passes through the crystal onto the chosen

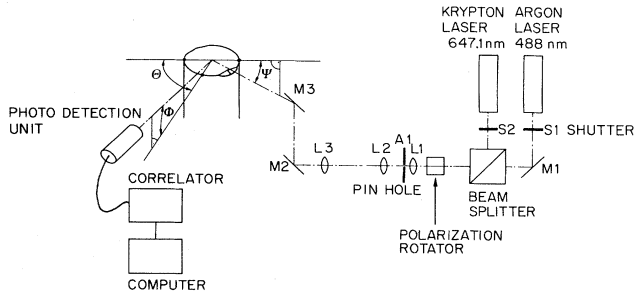

FIG. 3. Experimental setup.

area of the interface plane. The polarization and the angle of incidence Ψ are chosen such that the beam is totally reflected at the interface. Owing to the total reflection of the laser beam an evanescent wave results on the liquid side of the interface. This evanescent wave acts as primary beam. We did not use the inverse light pass where the laser beam enters from the liquid side since the strong Rayleigh scattering from the liquid would make the observation of the interface difficult.

The scattered light is observed from the liquid side under an inclination Φ of about 5° with respect to the facet plane. θ is the angle between the projection on the interface plane of the incident laser beam and the direction of observation. The detection system (Fig. 4) for the scattered light is almost the same as the one described by Haller.[12] It can be rotated around the axis of the growth tube. The interface is imaged by the lenses $L1$ ($f=100$ mm) and $L2$ ($f=40$ mm) on the circular aperture $A2$ ($\phi=0.25$ mm) which determines the scattering volume. The aperture $A1$ limits the range of accepted scattering angles and thus determines the size of the coherence speckles. The effective scattering volume can be inspected by eye using the removable mirror $M2$ and the corresponding eyepiece. A much larger surface area can be looked at using the mirror $M1$. The lens $L3$ ($f=30$ mm) focuses the light onto the sensitive area (approximately 5 mm^2) on the photocathode of the magnetically defocused photomultiplier tube (EMI 9813KB). The discriminator-preamplifier is described in Ref. 13. The photon counts are autocorrelated by a 128 channel multibit correlator (Malvern 7025) interfaced to a minicomputer (Minc11, Digital Equipment Corporation).

IV. EXPERIMENTAL RESULTS

We investigated the solid-liquid interface of crystals growing at velocities v_k between 0.2 and 0.8 μm/s along the [001] and [010] axes. Two different types of scattering have been observed at the interface. One shows a distinct anisotropy of the scattered intensity and an oscillating intensity autocorrelation function, the other is characterized by an isotropic scattered intensity and an exponentially decaying autocorrelation function. In the following the two types are named "Doppler scattering" and "diffusive scattering."

A. Doppler scattering

On the (001) and (010) facet of a growing salol crystal regions of about 0.5 mm^2 are found, where light is scattered by a surface structure. Since the normal components of the deviations from the ideally flat surface are negligible on the scale of the laser wavelength, the scattering may be treated as arising from a two-dimensional structure. As a consequence the projection of the scattering vector on the facet plane, $\vec{q}_{||}$, is the relevant parameter in the scattering experiment. By virtue of the generalized Patterson theorem the intensity measured at $\vec{q}_{||}$ is proportional to the Fourier transform of the spatial autocorrelation function of the scattering density. Our experiments show that the structure giving rise to the light scattering at the interface acts similarly to a moving imperfect line grating.

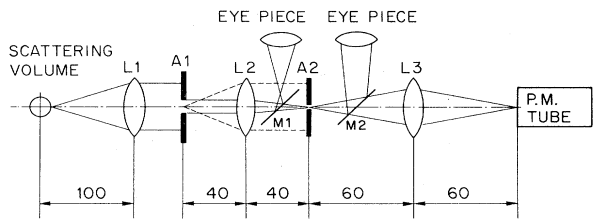

FIG. 4. Optics in front of the photomultiplier (dimensions in mm) L, lenses; M, mirrors; A, apertures.

1. Scattered intensity

We have observed diffraction peaks up to fourth order at low growth rates $v_k=0.2$ μm/s, whereas at $v_k=0.8$ μm/s only the first-order peak was found. The width of the peaks, arising from the imperfect spatial periodicity of the scattering system, corresponds to an angular variation of $\vec{q}_{||}$ of about 5°. With increasing growth velocity the diffraction peaks become less intense and their width increases slightly. Width and intensity of the diffraction peaks are not sufficiently reproducible to justify an analysis of the line shapes. A typical result for a crystal growing parallel to the [001] axis is shown in Fig. 5 where

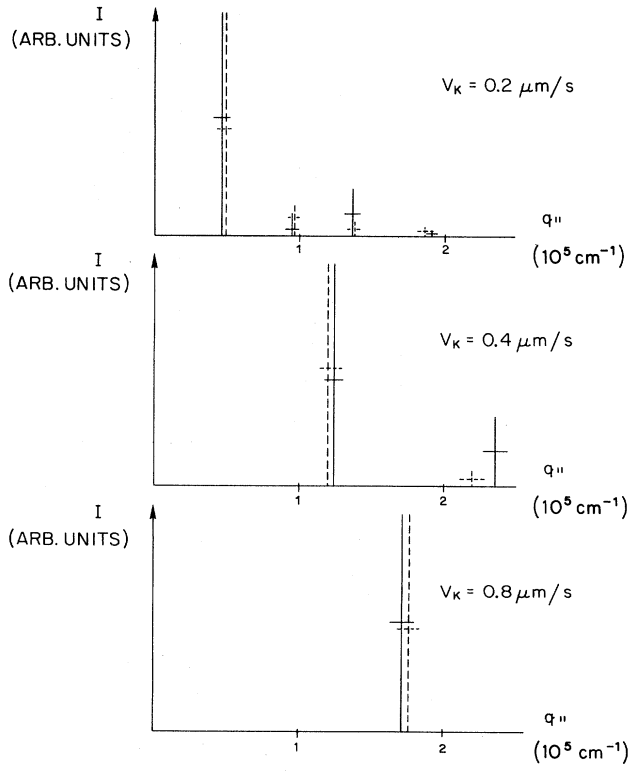

FIG. 5. Proof of Bragg reflection. Peak intensities vs $q_{||}$. Wavelength of the incident light: 488 nm (solid lines) and 647.1 nm (dashed lines). The horizontal bars mark the approximate width of the peaks.

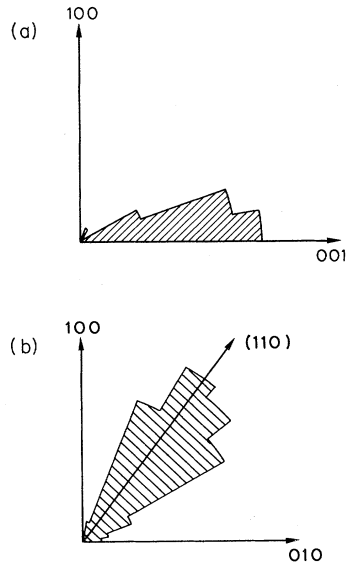

FIG. 6. Probability for the observation of nonzero scattering intensity for different orientations of $\vec{q}_{||}$. (a) Growth parallel to the [010] axis. (b) Growth parallel to the [001] axis.

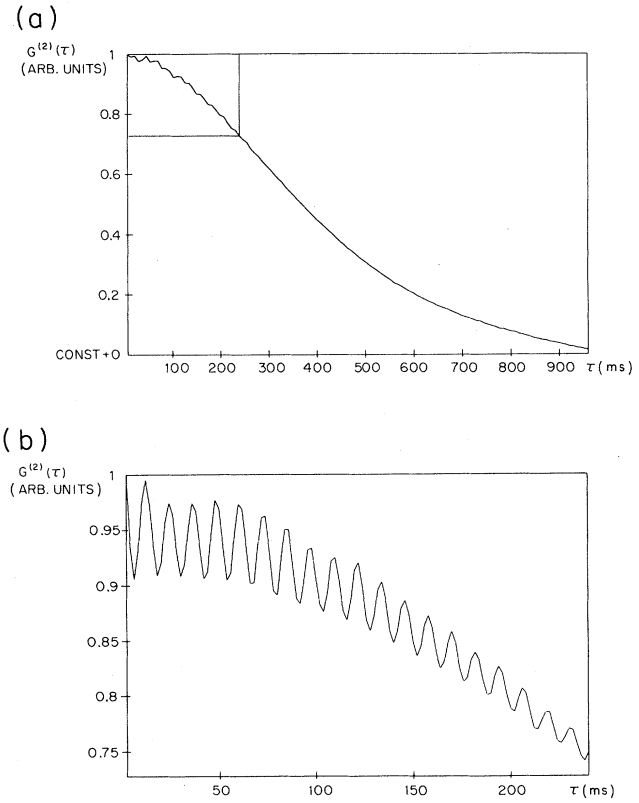

FIG. 7. Typical intensity autocorrelation function $g^{(2)}(\tau)$ in the case of Doppler scattering. (a) The nonoscillatory contribution. (b) Inset of (a) on an expanded scale showing the oscillations due to the Doppler-shifted component of the scattered light.

the peak intensity is plotted versus $q_{||}$ ($=|\vec{q}_{||}|$) for different growth velocities. We also find a substantial scattered intensity for $\vec{q}_{||}$'s of arbitrary length provided the orientation is the same as for the diffraction peaks. This intensity, which is evidently due to deviations from the periodicity of the "line grating," increases with growth velocity. At $v_k=0.2$ μm/s it is hardly detectable whereas it can be of the order of the peak intensity at $v_k=0.8$ μm/s.

The angular distribution of the $\vec{q}_{||}$'s for which scattering has been observed has a maximum along the [110] and [001] directions for growth parallel to the [001] and [010] axis, respectively (Fig. 6).

2. *Autocorrelation function*

The intensity autocorrelation function contains two contributions. One is oscillatory, the frequency of the oscillations being of the order of 100 Hz; the other, larger in amplitude, shows a bell-shape-like dependence on the correlation time τ. The amplitude of the nonoscillatory component is proportional to $1-\alpha\tau^2$ for $\tau \lesssim 0.3$ s and it is half its initial value for correlation times around typically 0.5 s (Fig. 7). We have not found a significant deviation from the behavior sketched above either upon changing growth velocity, growth direction, and scattering angle, or upon changing the wavelength of the incident laser beam. The oscillatory part in the autocorrelation function is due to the beat of a Doppler-shifted component of the scattered light with the unshifted component. This was verified by measuring the dependence of the oscillation frequency on the length of $\vec{q}_{||}$ which was changed by varying the scattering angle and the wavelength of the laser light. The frequency shift turned out to be proportional to $\vec{q}_{||}$ (Fig. 8). We thus conclude that the surface structure propagates parallel to $\vec{q}_{||}$ at a velocity v_s that is given by the ratio of the Doppler shift Ω to the length of the scattering vector $q_{||}$ ($v_s \ll c$)

$$v_s=\Omega/q_{||}=\Omega\frac{c}{2\omega_i n_s \cos\Psi \sin(\theta/2)} . \tag{4.1}$$

ω_i is the frequency of the illuminating laser beam and n_s ($\simeq 1.6$) is the refractive index of the crystal (for the geometry see Fig. 3). The experimentally determined velocities v_s are about 100 times larger than the growth velocity v_k of the crystal.

3. *Summary and results*

On the [010] and [001] facet of a growing salol crystal we found areas where light is scattered by a propagating line-grating-like surface structure. The observed diffraction peaks, which are more pronounced at low growth velocities than at high ones, permit the determination of the period d of the grating. Simultaneously we obtain the propagation velocity v_s of the structure from measurements of the Doppler shift.

Experimentally we found relations between v_s, d, and v_k (the growth velocity of the crystal). For growth along the (001) axis the dependence of d on v_s can be fitted by

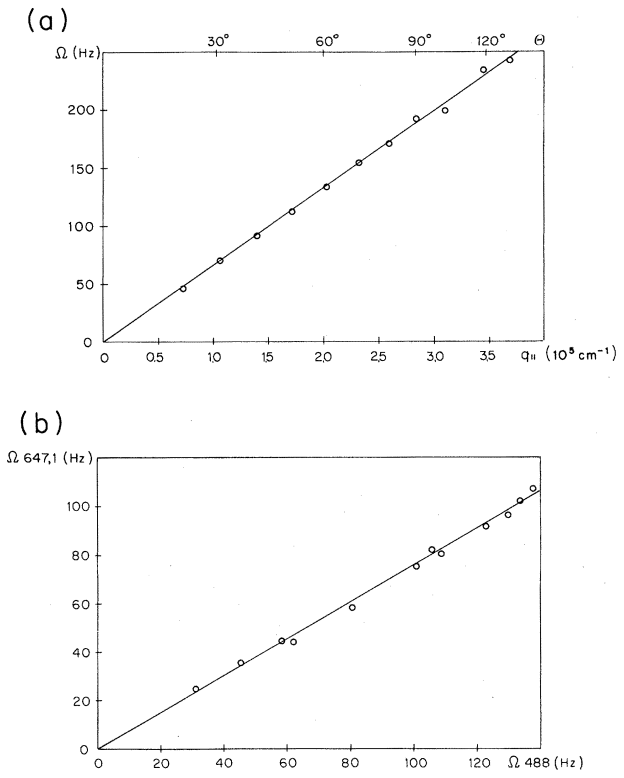

FIG. 8. Proof of Doppler shift. (a) Doppler shift Ω vs $q_{||}$. The magnitude of $q_{||}$ was varied with the scattering angle θ (wavelength of the incident light, 488 nm, growth parallel to the [001] axis at 0.5 μm/s). (b) Doppler shift $\Omega_{647.1}$ measured at a wavelength of the incident laser beam of 647.1 nm vs the Doppler shift Ω_{488} measured at a wavelength of 488 nm. The slope of the solid line is equal to the wavelength ratio (488 nm)/(647.1 nm) [crystal and growth velocity are the same as in (a)].

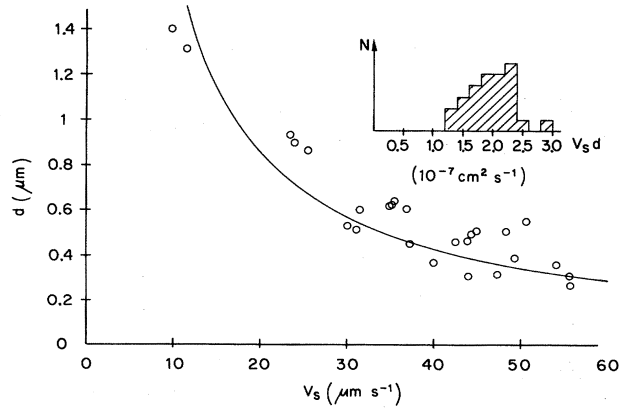

FIG. 9. Period d vs propagation velocity v_s of the line-grating-like structure for growth of the crystal parallel to the [001] axis. The solid line represents the fit $d=C/v_s$ with $C=1.8\times10^{-7}$ cm^{2}s^{-1}. Inset: Histogram of the measured products $v_s d$.

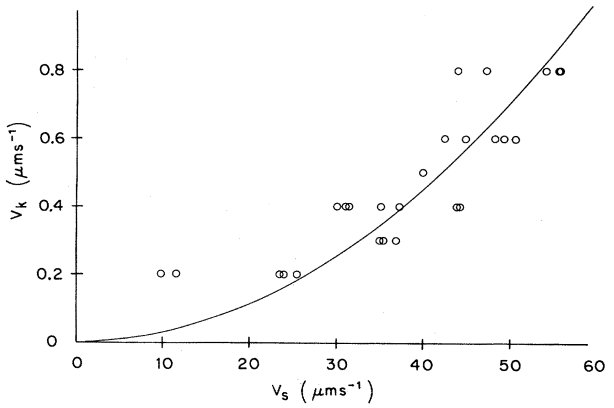

FIG. 10. Growth velocity v_k vs propagation velocity v_s for growth parallel to the (001) axis. Solid line: $v_k=\alpha v_s^2$ ($\alpha=3$ cm^{-1}s).

$$d=C/v_s \tag{4.2}$$

with $C=(1.8\pm0.5)\times10^{-7}$ cm^{2}s^{-1} (Fig. 9). The dependence of v_k on v_s can be fitted by

$$v_k=Rv_s^2 \tag{4.3}$$

with $R=3\pm0.5$ cm^{-1}s (Fig. 10). Typical values for d and v_s are 0.4 μm and 40 μm/s, respectively, at a growth rate of 0.5 μm/s.

Experiments on crystals growing along the (010) axis are more difficult because of the less favorable optical conditions. The available experimental data do not permit us to establish relations analogous to (4.2) and (4.3). Nevertheless, we can say that for a given growth velocity the period d is about the same as for growth along the (001) axis, whereas the propagation velocity v_s is about double.

B. Diffusive scattering

In the range of the investigated growth velocities $v_k \leq 0.8$ μm/s diffusive scattering has only been observed on the (010) facet of the salol crystals. After the initiation of growth Doppler scattering is seen at first. If a critical growth velocity, which varies in different experiments between 0.2 and 0.8 μm/s, is exceeded intense light scattering is observed in an area of a few mm^2 near the center of the facet. The scattered intensity shows a hysteretic behavior as a function of growth velocity. This diffusive scattering persists even if the growth velocity is reduced below the critical velocity for the onset of scattering and it does not disappear unless the facet begins to melt. With the onset of scattering the intensity increases with time (the growth velocity is kept constant) until a steady state is reached after about 30 min. No correlation between the scattered intensity and the growth velocity has been found.

We measured the dependence of the scattered intensity on the angle of incidence Ψ of the laser beam on the interface (see Fig. 3). The intensity rises rapidly as Ψ approaches the critical angle of total reflection (Fig. 11). This indicates that the scattering does not arise from fluc-

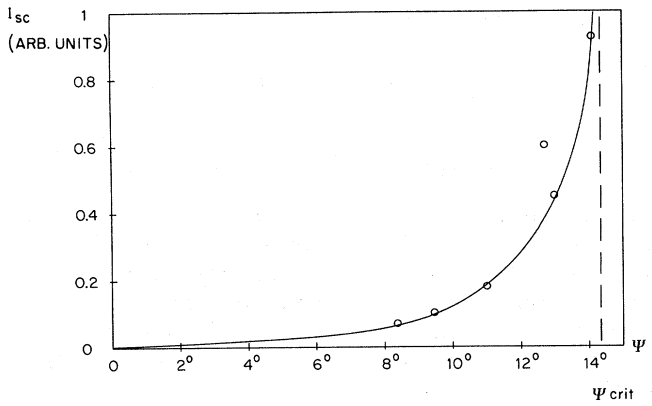

FIG. 11. Scattered intensity vs angle of incidence Ψ (Ψ_{crit} is the critical angle of total reflection; scattering angle $\theta=60°$). The solid line is a guide to the eye.

tuations in the crystalline phase. (If it would, the laser beam reflected at the interface would act as the incident wave and not the evanescent wave on the liquid side. Thus the illumination of the scattering volume would be almost independent of Ψ and no increase would be expected at the approach of the critical angle.) As a rule we also found an increase of the scattered intensity with decreasing length of the scattering vector.

The intensity autocorrelation function can be fitted by a single exponential. The linewidth Γ is proportional to the square of the scattering vector $\vec{q}$ (Fig. 12) which was nearly parallel to the interface in all experiments (taking the evanescent wave as the incident wave). The measured values of the $\vec{q}$ independent quantity $\Gamma/\sin^2(\theta/2)$ are subjected to a large scatter. Data obtained from five different crystals yield an averaged $\Gamma/\sin^2(\theta/2)$ of 160 ± 40 rad/s. No statistically significant dependence either on the growth velocity or on the orientation of $\vec{q}$ in the facet plane has been found.

V. DISCUSSION OF THE DIFFUSIVE SCATTERING

In the paper by Böni *et al.*[8] it has been shown that an interface layer of thickness of the order of a few micrometers builds up at the solid-liquid interface of a growing ice crystal. In this layer Rayleigh scattering is more than 2 orders of magnitude more intense than in bulk water at 0 °C. The diffusion constant D_i describing the decay of density fluctuations in the layer is 10^5 times smaller than the thermal diffusivity in water, and the fluctuations giving rise to scattering are isotropic. It has been suggested that D_i might describe Frenkel's "structure diffusion."

A. Interface layer

In Ref. 8 the existence of an interface layer is inferred from two observations.

(1) The diffusion constant D_i is independent of the orientation of the scattering vector. Therefore, it can be concluded that the thickness of the layer is at least $2\pi/q_m$, where q_m is the shortest scattering vector realizable in the experiment.

(2) The measured intensity of the scattered light can be interpreted assuming that the scattering originates in a three-dimensional interface layer which acts like a leaky wave guide for the incident laser beam.

Unfortunately the salol data are not sufficiently complete to permit an interpretation along the same lines. Nevertheless, the measurement of the scattered intensity as a function of the angle of incidence Ψ of the illuminating laser beam (see Sec. IV B and Fig. 11) suggests that the scattering at the solid-liquid interface of salol also arises from fluctuations in a layer of finite thickness.

For the sake of argument we consider first a model in

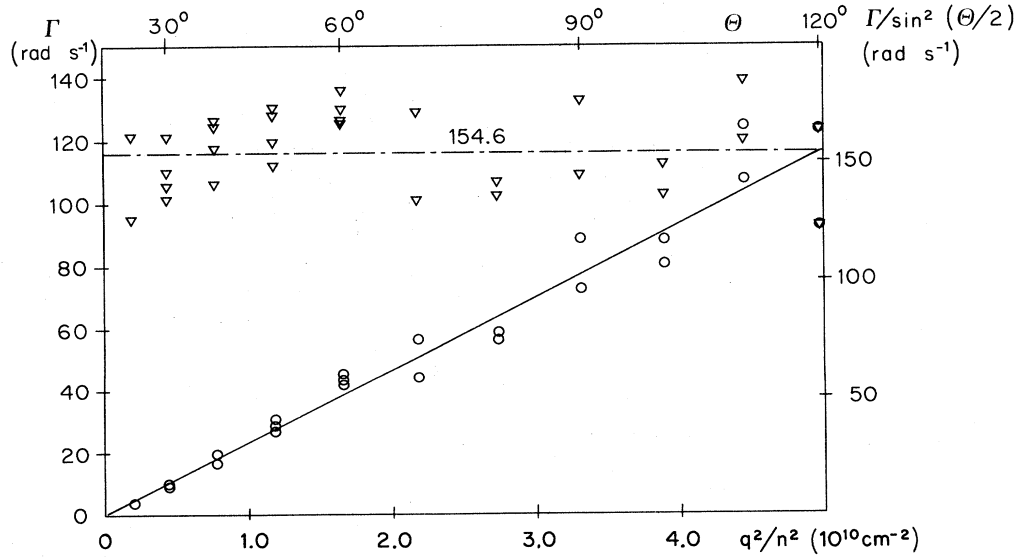

FIG. 12. Linewidth Γ (circles) and q-independent quantity $\Gamma/\sin^2(\theta/2)$ (triangles) vs the square of the scattering vector. (n is the refractive index of the crystal.)

which the light is scattered off a sharp corrugated interface that fluctuates about a mean plane with amplitudes small compared to the wavelength of light (corrugated interface model of Güttinger *et al.*[7]). This model yields a q^2 dependence of the linewidth and also predicts the right order of magnitude of the diffusion constant D_i (Ref. 7) as long as the scattering vector is parallel to the interface. As shown in Ref. 8 the intensity scattered by a corrugated interface is roughly proportional to the square of the electric field of the evanescent wave at the interface.

In a second model (interface layer model) we assume a statistically homogeneous interface layer in which the evanescent wave propagates. The thickness of the layer shall be larger than the wavelength of the incident light. One expects that the scattered intensity due to density fluctuations in the layer is proportional to the integral over the scattering volume of the Poynting vector associated with the evanescent wave.

In order to calculate the electric field $\vec{E}_e$ of the evanescent wave we make for either model three assumptions.

(1) The boundary between the crystal and the noncrystalline phase (melt or interface layer) is sharp.

(2) The refractive index of the noncrystalline phase at the interface is equal to the refractive index of liquid salol at the melting temperature.

(3) The interface is flat on the scale of the laser wavelength.

With these assumptions $\vec{E}_e$ can be determined using the Fresnel equations. Taking into account that in the experiment the polarization of the reflected laser beam is parallel to the plane of incidence we obtain

$$\vec{E}_e(x,y,z,t)=\vec{e}_z E_0 \exp(ik_x x - i\omega t - k_z z) , \tag{5.1}$$

$$E_0=\frac{2n\sin\Psi}{n^2\sin\Psi+(n^2-\cos^2\Psi)^{1/2}}E_i . \tag{5.2}$$

The z axis has been chosen perpendicular to the interface plane with the corresponding unit vector $\vec{e}_z$ pointing into the liquid, and the x axis points along the propagation direction of the evanescent wave. E_i is the electric field strength of the incident wave, n is the ratio of the refraction index of the melt to the refractive index of the crystal, and Ψ is the angle of incidence as defined in Fig. 3. With k_x we denote the projection of the incident wave vector k_i on the interface plane

$$k_x=k_i\sin\Psi , \tag{5.3}$$

where k_i is given by

$$k_i=\frac{2\pi}{\lambda}n_s . \tag{5.4}$$

λ is the vacuum wavelength of the incident light and n_s is the refractive index of the crystal. The imaginary part k_z of the wave vector of the evanescent wave is equal to

$$k_z=k_i(\cos^2\Psi-n^2)^{1/2} . \tag{5.5}$$

For the *corrugated interface model* we now obtain for the scattered intensity (in the case $\cos\Psi > n$)

$$\begin{aligned} I_{sc} &\propto \int_\Omega dx\,dy \vec{E}_e(z=0)\vec{E}_e^*(z=0) \\ &= \frac{4n^2\sin^2\Psi}{(n^4-1)\sin^2\Psi-(n^2-1)}\int_\Omega dx\,dy\,|E_i|^2 \\ &= K\frac{4n^2\sin^2\Psi}{(n^4-1)\sin^2\Psi-(n^2-1)} , \end{aligned} \tag{5.6}$$

Ω is the interface area which is imaged onto the photocathode of the detector. Since in the experiment the aperture A_2 in the image plane of the optical system in front of the detector (Fig. 4) was chosen sufficiently large to accept the whole illuminated interface area the integral in Eq. (5.6) is independent of Ψ and we can replace it by a constant K.

For the scattered intensity for the *interface layer model* one can write

$$I_{sc} \propto \int_\Omega dx\,dy \int dz\,|\vec{S}(z)| . \tag{5.7}$$

Maxwell's equations yield for the Poynting vector $\vec{S}(z)$

$$\vec{S}(z)=\vec{e}_x\frac{1}{8\pi}\frac{k_i}{\omega}\cos\Psi E_0 E_0^* \exp(-2k_z z) \quad (z\geq 0) . \tag{5.8}$$

Dropping all factors in (5.8) that are independent of Ψ and z we finally have

$$\begin{aligned} I_{sc} &\propto \frac{4n^2\sin^2\Psi}{(n^4-1)\sin^2\Psi-(n^2-1)}\cos\Psi \\ &\quad \times \int dz \exp(-2k_z z)\int_\Omega dx\,dy\,|E_i|^2 . \end{aligned} \tag{5.9}$$

The integration over z extends over the thickness δ of the interface layer. As long as $1/k_z$ is smaller than δ we can extend the integration to infinity without introducing large errors. Writing again K for the integral over Ω we obtain

$$I_{sc} \propto K\frac{4n^2\sin^2\Psi}{(n^4-1)\sin^2\Psi-(n^2-1)}\frac{\cos\Psi}{2k_z} . \tag{5.10}$$

In order to decide which model applies we plot the measured intensity for the angle Ψ versus the calculated intensity for the same angle Ψ. The points in the plot based on the "correct" model should lie on a straight line through the origin. The result is shown in Fig. 13. Clearly the layer model is to be preferred. Even for the largest angle of incidence $\Psi_{max}=14.1°$ (see Fig. 11) for which the intensity was measured relation (5.10) can be applied. Therefore, one can conclude that the condition $1/k_z<\delta$ holds for all angles $\Psi\leq 14.1°$. Thus we obtain a lower limit for the layer thickness

$$\delta \geq \frac{1}{k_z(\Psi_{max})}=\frac{1}{k_i(\cos^2\Psi_{max}-n^2)^{1/2}} . \tag{5.11}$$

With the wavelength of the incident light $\lambda=488$ nm, the refractive index of the salol crystal $n_s\approx 1.6$ and $n^2=\cos^2\Psi_{crit}$, where $\Psi_{crit}=14.3°$ is the critical angle for total reflection, we obtain a lower limit for δ of 1 μm. This value is of the same order of magnitude as the lower limit of the interface layer thickness measured in the ice-water experiment.[8]

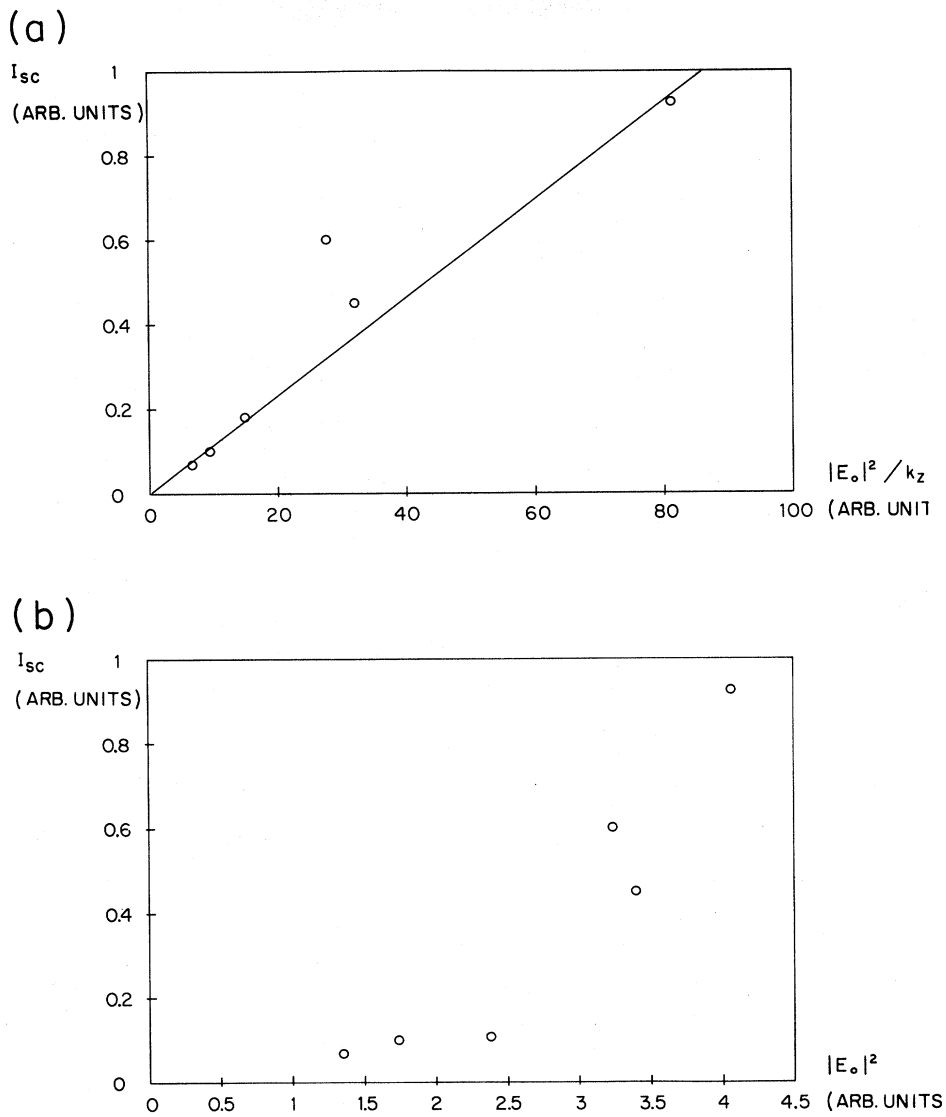

FIG. 13. Measured intensity for different angles Ψ vs calculated intensity for the same angles. (a) Interface layer model (the straight line serves as a guide to the eye). (b) Corrugated interface model.

B. The linewidth of the scattered light

We assume that the light is scattered in a layer of a thickness of a few μm. Models of this layer must be compatible with the observation that the spectrum of the scattered light is a single Lorenzian with a linewidth Γ proportional to the square of the scattering vector. We consider first a model where we assume that salol crystallites are suspended in the melt close to the interface. In a second model we assume that the layer may be interpreted as a liquidlike continuum in which the light is scattered by density fluctuations.

1. Suspended crystallites

The linewidth Γ of light scattered from noninteracting particles undergoing Brownian motion in a liquid is given by (see, e.g., Ref. 14)

$$\Gamma = Dq^2 , \tag{5.12}$$

where D is the diffusion constant of the particles in the liquid. D can be related to the so-called hydrodynamic radius r_h of the particles by virtue of the Stokes-Einstein equation (η is the viscosity of the liquid)

$$D = \frac{k_B T}{6\pi\eta r_h} . \tag{5.13}$$

Since the measured intensity autocorrelation function can be fitted by a single exponential the particles are monodisperse. Thus we rule out that the light scattering arises from contaminations accumulated in front of the interface during zone refining.

With Eq. (5.12) and

$$q = 2k_x \sin(\theta/2) \tag{5.14}$$

we obtain from the measured values of $\Gamma/\sin^2(\theta/2)$ (see Sec. IV B) a diffusion constant D of $(1.0\pm0.25)\times10^{-9}$ cm^2s^{-1} corresponding to a hydrodynamic radius r_h of 275 nm. This value of r_h happens to be equal to the critical radius r_c of a spherical salol crystallite that is in equilibrium with the melt at an undercooling ΔT of ~0.4 K. The undercooling of the liquid salol at the interface is of the same order of magnitude in our experiments and one is tempted to assume that small crystal nuclei of radius r_h are spontaneously created in the interface layer. However, the formation probability of such a nucleus is vanishingly small since the required energy is, according to classical nucleation theory, 6 orders of magnitude larger than the energy of thermal fluctuations. Furthermore, it is difficult to see why nuclei of the critical size should persist in this layer. Therefore, we reject the model of diffusing nuclei.

2. *Continuum model*

We assume that at the solid-liquid interface of a growing salol crystal a liquidlike interface layer builds up where the density fluctuations have a correlation length ξ which is very large compared to the mean distance between the molecules. Hence Rayleigh scattering is by orders of magnitude more intense in this layer than in the bulk liquid as is borne out by the experiment. In the hydrodynamic limit, $q\xi \ll 1$ ($\vec{q}$ is the scattering vector) the linewidth of the scattered light is given by

$$\Gamma = D_i q^2 . \tag{5.15}$$

D_i, which for simple fluids is equal to the thermal diffusivity, is now a diffusion constant describing the decay of entropy fluctuations.[15] Our measured value, $D_i \sim 10^{-9}$ cm^2s^{-1}, is 6 orders of magnitude smaller than the thermal diffusivity of liquid salol. According to ideas of Bilgram[16] the formation of "bonds" between molecules in the layer could account for the slowing down of the decay of the fluctuations.

Tentatively we assume that the interface layer consists of a hypothetical "bonded" phase and that this phase can continuously transform into the liquid phase. We further assume that the energy required to break a "bond" is so small that fluctuations of the thermal energy give rise to large fluctuations in the degree of "bonding" to which one can assign an order parameter. Assuming an Ornstein-Zernike form for the correlation function of the order parameter fluctuations Kawasaki has shown[17] that in the hydrodynamic limit the correlation length ξ and the diffusion constant D_i describing the decay of the fluctuations are related according to the Stokes-Einstein equation

$$D_i = \frac{k_B T}{6\pi\eta^* \xi} , \tag{5.16}$$

where η^* is an effective viscosity which is about 1.3 times the macroscopic shear viscosity η.[18] Inserting our measured D_i and the effective viscosity of liquid salol η_s^* we obtain a correlation length ξ of ~200 nm. Hence we have $q\xi > 1$ in our experiments, and therefore the equations valid in the hydrodynamic limit become meaningless. Theory of critical fluctuations[17] predicts that in the limit $q\xi \gg 1$ the linewidth is proportional to q^3, the departures from the q^2 dependence becoming already noticeable at $q\xi \simeq 1$. Since experimentally the q^2 dependence of the linewidth is well established critical fluctuation theory cannot be used to interpret the measured linewidth, unless one assumes an effective viscosity η^* in the layer which is at least an order of magnitude larger than η_s^*.

VI. DISCUSSION OF THE DOPPLER SCATTERING

We interpret the line-grating-like structure, giving rise to the observed Doppler shifted light scattering (see Sec. IV A) in terms of roughly equidistant growth steps moving across the facet. We assume that the source of these steps are screw dislocations intersecting the interface. The step originating at the screw dislocation spirals around the screw axis during crystal growth. Far from the center of the spiral the radial step velocity and the step spacing are constant so that an equidistant propagating step pattern is established. According to this picture we have measured *in situ* the propagation velocity v_s and the spacing d of these growth steps. During a time d/v_s the crystal facet advances by a step height h. Using the macroscopic growth velocity v_k one therefore has

$$h = \frac{v_k}{v_s} d . \tag{6.1}$$

Our simultaneous measurements of v_k, v_s, and d yield for the height of the growth steps on the (001) facet $h = 6\pm2$ nm. This value is about 2.5 lattice constants and independent of the growth velocity.

Growth spirals on facets of crystals growing from the vapor phase, from the solution, or from the melt have been observed by many authors. In the earliest experiments the crystal facets were investigated by means of standard microscopy. For example, growth spirals on solution-grown salol crystals were found by Amelinckx.[19] Facets of vapor-grown crystals are usually investigated under the electron microscope. Bethge,[20] using a gold decoration technique, studied the dynamics of growth spirals on NaCl crystals. He found that the step velocity increases with the step spacing as long as the velocity is below a certain limit. Recently optical phase contrast microscopy was applied by Tsukamoto[21] to study *in situ* the growth patterns of CdI_2 crystals grown from solution. The phase contrast technique allows a direct measurement of the step height. Tsukamoto showed that growth spirals with a step height of molecular dimensions comprising more than 10 turns can evolve from isolated screw dislocations.

As early as 1949 Frank[22] pointed out that the observed high growth rates at low supersaturations cannot be explained by standard nucleation theory (e.g., Ref. 4) and proposed that screw dislocations intersecting the interface would provide a permanent source of growth steps. As a consequence the growth rate is determined by the velocity at which steps advance on the facet and not by the nucleation rate of new steps. Burton, Cabrera, and Frank[5] treated the microscopic structure as well as the advance rate of growth steps. They assumed that the molecules arrive at the step by surface diffusion only. In a recent

more general theory[23] Van der Eerden solved the coupled surface and volume diffusion problem in order to calculate the advance rate of the steps.

For the discussion of our measurements of the dynamics of growth steps on the [001] facet of salol crystals we follow ideas developed in Ref. 5. Our calculation of the step spacing and the step velocity is based on the following assumptions.

(1) The origin of the steps are screw dislocations. The component of the Burgers vector perpendicular to the facet is of the same length as the measured step height.

(2) The solid-liquid surface tension σ_{sl} depends upon the indices of the crystal face. It has a minimum for $(11l)$ faces. Therefore, the steps are perpendicular to these directions [as suggested by Fig. 6(b)] and the growth spiral has a parallelogramlike shape (Fig. 14).

(3) The diffusion of the latent heat generated at the steps is so fast that it does not limit the growth velocity. Taking typical values for the step spacing (500 nm), the step velocity (40 μm/s), and the thermal diffusivity (10^{-3} cm^2/s) it can be shown that by the time a heat pulse has spread over a distance of one step spacing the steps themselves have advanced by less than 1 Å. Therefore, we can assume that the temperature field in the rest frame of a step is static.

(4) Since we are interested in crystal growth from the melt and not from the vapor phase, we assume that the molecules enter the step directly from the melt and neglect the contribution due to surface diffusion.

(5) We assume that the molecules attach at each lattice site of the step with equal probability thus producing a rough step. According to Wilson[2] and Frenkel[3] the propagation velocity of the steps is then determined by the difference of the rate of molecules arriving at the step due to self-diffusion in the melt and the rate of molecules leaving the step due to thermal activation. Hillig and Turnbull[24] used a similar approach and arrived at a square law dependence of the macroscopic growth velocity v_k of the crystal on the undercooling ΔT of the melt for growth by the screw dislocation mechanism.

(6) For further simplification we use the Kossel model to describe the salol crystal. The molecules are considered to be cubes. Accordingly we assume that the (100) and (010) axes of the unit cell are of equal length.

First, we write down the net rate q_∞ at which the molecules are incorporated into the crystal lattice at a straight step of infinite length (the system is assumed to be in local equilibrium, see, e.g., Ref. 25)

$$q_\infty = \frac{D}{a^2}\left[1-\beta\exp\left[-\frac{\Phi_\infty}{k_B T}\right]\right] . \tag{6.2}$$

Φ_∞ is the activation energy to bring a molecule from the crystalline state into the liquid state. (Following Wilson and Frenkel Φ_∞ is equal to the latent heat of fusion per molecule.) T is the temperature of the melt at the step, D is the self-diffusion constant in the melt, and a is the corresponding jump length which we identify with a mean molecular distance by setting

$$a = \left[\frac{m}{\rho_l N}\right]^{1/3} . \tag{6.3}$$

With m, ρ_l, and N we denote the molecular weight, the density of the liquid, and the Avogadro number, respectively. β is the ratio of the jump frequency of the molecules in the solid to the jump frequency in the liquid. Its value is determined by the equilibrium condition $q_\infty = 0$ at the melting temperature T_m

$$\beta = \exp(\Phi_\infty / k_B T_m) . \tag{6.4}$$

Next one considers steps of a length l which form the boundary of a square nucleus of height h. In this case the crystallization rate q_l is smaller than q_∞ for a given undercooling $\Delta T = T_m - T$ since, at the same time a step advances by a distance Δx, the edge surface of the nucleus is increased by the amount $2\,\Delta x\, h$. Therefore, the activation energy is reduced by the additional surface energy divided by the number of added molecules, and one has to replace Φ_∞ in Eq. (6.2) by the expression

$$\Phi_l = \Phi_\infty - 2\frac{\sigma_{sl} a_s^3}{l} . \tag{6.5}$$

a_s, the mean distance between the molecules in the crystal, can be calculated according to Eq. (6.3) by exchanging the density of the liquid, ρ_l, by the density of the solid. Since the density difference is small we put a_s equal to a. Finally one obtains for the crystallization rate q_l

$$q_l = \frac{D}{a^2}\left\{1-\exp\left[-\frac{\Phi_\infty \Delta T}{k_B T T_m}\left[1-\frac{l_{crit}}{l}\right]\right]\right\} . \tag{6.6}$$

l_{crit} is given by

$$l_{crit} = 2\frac{\sigma_{sl}}{S_f \Delta T} . \tag{6.7}$$

In (6.7) we equated the entropy of fusion S_f with $\Phi_\infty/(T_m a^3)$. From Eq. (6.6) it can be seen that the steps cannot propagate unless their length exceeds l_{crit}.

Equation (6.6) and the requirement that the steps are perpendicular to the directions of the minimum surface tension together determine the dynamics of the growth spiral. We do not attempt to solve the problem rigorously and restrict ourselves to calculate the step velocity v_s far away from the screw dislocation and to estimate the distance between two successive steps.

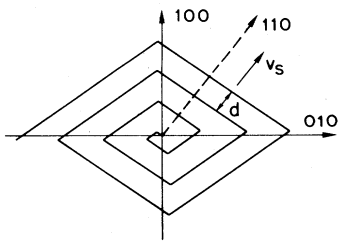

FIG. 14. Schematic representation of a growth spiral on the (001) facet.

We first consider a facet at zero undercooling of the melt intersected by a single screw dislocation intersecting. The free energy is minimized by a configuration where a single straight step originates at the intersection point. Upon lowering the temperature this step advances at a velocity v_s equal to the product of the rate q_∞ and the mean distance by which a surface element a^2 of the step advances upon attachment of one molecular cube. Up to first order in ΔT one obtains

$$v_s = \frac{D}{a}\frac{\Phi_\infty \Delta T}{k_B T T_m} . \tag{6.8}$$

During the time the first step advances a second straight step is created linking the first one with the step source (Fig. 15). After a time l_{crit}/v_s the second step has reached the critical length and starts itself to advance at a velocity v_l which now depends on the length of the step

$$v_l = v_s \left[1 - \frac{l_{\text{crit}}}{l}\right] . \tag{6.9}$$

As a consequence a third step is created. This procedure perpetuates *ad infinitum* thereby creating the characteristic growth spiral.

For an approximate calculation of the distance between two parallel successive steps of the spiral we use instead of (6.9)

$$v_l = \begin{cases} 0 & \text{for } l \le l_{\text{crit}} \\ v_s & \text{for } l > l_{\text{crit}} . \end{cases} \tag{6.10}$$

The step spacing is then four times the critical length. A more accurate calculation (see Appendix A) yields for the step spacing far from the center of the spiral

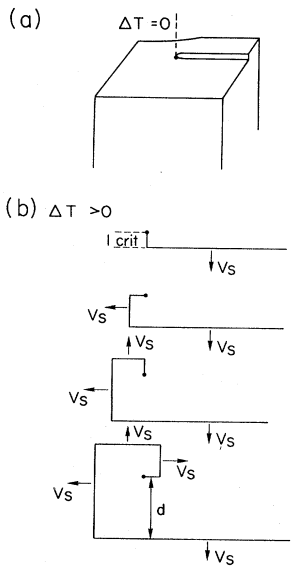

FIG. 15. (a) Screw dislocation (dashed line) intersecting the facet. At zero undercooling ΔT of the melt it gives rise to an infinitely extended straight step. (b) Schematic representation of the evolution of a growth spiral.

$$d \approx 8.6 l_{\text{crit}} \approx 8.6\times 10^{-5}\ \text{cm K}^{-1}\frac{1}{\Delta T} . \tag{6.11}$$

In our experiments the undercooling of the melt at the interface is of the order of 0.5 K. Thus the agreement between the calculated and the measured step spacing is satisfactory.

So far we have neglected the influence of the stress field in the vicinity of the screw dislocation. It can be shown[26] that the effect of this field can be taken into account by substituting the bracket in the exponential of equation (6.6) by

$$1 - \frac{l_{\text{crit}}}{l} - \frac{\mu \vec{b}^2 l_{\text{crit}}}{8\pi^2 \sigma_{\text{sl}} r^2} . \tag{6.12}$$

μ is the shear modulus, $\vec{b}$ the Burgers vector, and r the distance from the dislocation. We can define a radius of influence r_D of the stress field by

$$r_D = \left[\frac{\mu \vec{b}^2 l_{\text{crit}}}{8\pi^2 \sigma_{\text{sl}}}\right]^{1/2} \approx 3.7\times 10^{-6}\ \text{cm} . \tag{6.13}$$

Inserting for $|\vec{b}|$ the measured step height we find that r_D is an order of magnitude smaller than the measured step spacing. Hence for our purposes we may neglect the corrections due to the stress close to the screw dislocation.

From Eqs. (6.7), (6.8), and (6.11) it follows that the product $C = v_s d$ does not depend upon the undercooling ΔT. Thus one expects that it does not depend upon the growth rate v_k either. This is in agreement with experiment. The above calculations yield

$$C = 8.6 v_s l_{\text{crit}} = 17.2 D \frac{\sigma_{\text{sl}} a^2}{kT} . \tag{6.14}$$

Since the constant of self-diffusion D of liquid salol is not known reliably we calculate it by means of the Stokes-Einstein equation. Inserting a molecular radius $a/2$ and the macroscopic shear viscosity η we obtain

$$C = 17.2\frac{\sigma_{\text{sl}} a}{3\pi\eta} = 2.92\times 10^{-5}\ \text{cm}^2\text{s}^{-1} . \tag{6.15}$$

This value is 2 orders of magnitude larger than the one obtained from the experiment (Fig. 9). In order to explain this discrepancy one has to scrutinize the crucial points (4) and (5) of the assumptions underlying the calculation of the growth rate v_s.

(1) The assumption that the step surface is rough may be wrong. However, even if the steps were facets, the growth rate would not be reduced by a factor of 160. The steps of the observed height contain about 8—10 molecular layers. Therefore, there is always an edge nearby that can act as a nucleation site, and one would expect the growth rate to be lower by a factor of 8—10 at most.

(2) The dynamics of the transport of the molecules towards the steps are assumed to be determined by the constant of self-diffusion in the liquid. However, they could be much slower. One might consider a model in which the advancing steps are surrounded by an interface layer similar to the one discussed in Sec. V. If we naively insert for D the measured D_i we calculate a constant C of

3.6×10^{-8} cm^{2}s^{-1}, which is only five times smaller than the experimental value. However, if the transport kinetics at the solid-liquid interface are much slower than in the bulk liquid one would also have to consider the current of molecules entering the step by surface diffusion. The fact that this contribution was neglected might account for the underestimation of the constant C.

VII. CONCLUSIONS

At the solid-liquid interface of a growing salol crystal two dynamical processes are observed which can be distinguished by the scattered light.

(1) For the first process the light scattering can be interpreted as arising from density fluctuations in an interface layer of a thickness of the order of 1 μm. This process is similar to the one observed at the ice-water interface.[7,8] The measured Rayleigh linewidths yield a diffusion constant for the decay of fluctuations in the layer, D_i, of $\approx10^{-9}$ cm^{2}s^{-1}. This value is 6 orders of magnitude smaller than the thermal diffusivity of liquid salol, which determines the decay of entropy fluctuations in the bulk melt. One is tempted to explain the observed slow kinetics in this interface layer in terms of a critical phenomenon. However, theoretical predictions and experimental results disagree unless one assumes that the effective viscosity η^* in the Stokes-Einstein equation, relating D_i and the correlation length ξ of the fluctuations, is at least 10 times larger than the shear viscosity of liquid salol.

(2) In the second process which has not been observed at the ice-water interface light is scattered by a line-grating-like surface structure. We interpret this structure in terms of almost equidistant growth steps advancing on the crystal facet. In the experiments we measure *in situ* simultaneously the step velocity v_s and the step spacing d at fixed values of the growth velocity v_k of the crystal. We find that the product $v_s d = C$ has a value of $(1.8\pm0.4)\times10^{-7}$ cm^{2}s^{-1} which is independent of v_k. For the step height $h = v_k d/v_s$ we obtain values of the order of 2.5 lattice constants. If we assume that the steps originate from growth spirals, which emanate from the intersection points of screw dislocations with the crystal facet, the measured step spacing is in agreement with calculations based on ideas of Burton, Cabrera, and Frank.[5] These calculations predict that C is independent of the undercooling of the melt and thus one expects that C does not depend on growth rate v_k either. However, the measured value of the constant C is 2 orders of magnitude smaller than the value calculated under the assumption that the molecules reach the steps by self-diffusion in the melt. This discrepancy is a hint that the advancing steps border at an interface layer in which the transport of the molecules towards the steps is much slower than in the melt. Whether this layer is identical with the one discussed under (1) is an open question.

ACKNOWLEDGMENTS

The authors acknowledge the collaboration of M. Wächter, K. Baumann, and P. Böni during the experiments. We thank P. Seiler from the Laboratory for Organic Chemistry of the Eidgenössische Technische Hochschule (Zürich) for the structure determination of salol and H. Arend for a critical reading of the manuscript. This work was supported by the Swiss National Science Foundation.

APPENDIX A: ESTIMATE OF THE STEP SPACING FAR FROM THE CENTER OF THE SPIRAL

We consider a rectangular growth spiral (Fig. 16). First we calculate the time lag Δt between the onset of the propagation of the nth step and the $(n+4)$th step (i.e., the next step propagating in the same direction as the nth). At a time t_n the nth step shall have reached the critical length $l_{\rm crit}$. It then begins to propagate at a velocity v_n thereby creating the $(n+1)$th step. According to Eq. (6.9) $v_n(t)$ is

$$v_n(t)=v_s\left[1-\frac{l_{\rm crit}}{l_n(t)}\right] \quad (t>t_n)\ . \tag{A1}$$

The length of the nth step, $l_n(t)$, is given by

$$l_n(t)=\int_{t_n}^{t} v_{n-1}(t')dt' \quad (t_n\le t\le t_{n+1})\ . \tag{A2}$$

At the time t_{n+1}, defined by $l_{n+1}(t_{n+1})=l_{\rm crit}$ or

$$l_{\rm crit}=\int_{t_n}^{t_{n+1}} v_n(t')dt' \tag{A3}$$

the $(n+1)$th step starts to advance. For an approximate calculation of t_{n+1} we replace in (A2) the propagation velocity of the $(n-1)$th step v_{n-1} by its maximum value v_s. Hence $l_n(t)$ can be written down explicitly:

$$l_n(t)=l_{\rm crit}+v_s(t-t_n) \quad (t_n\le t\le t_{n+1})\ . \tag{A4}$$

Inserting (A4) into (A1) we obtain

$$l_{\rm crit}=v_s(t_{n+1}-t_n) - l_{\rm crit}\ln\left[1+\frac{v_s(t_{n+1}-t_n)}{l_{\rm crit}}\right]\ . \tag{A5}$$

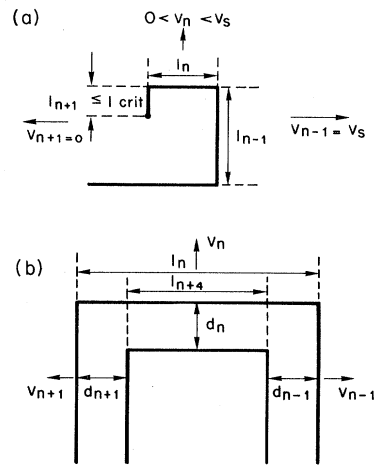

FIG. 16. (a) Center of the model growth spiral. (b) Steps far from the center.

TABLE II. Some physical constants of solid and liquid salol.

Solid		
density	$\rho_s = 1.321$ q cm^{-3} (25 °C)	Ref. 27
thermal conductivity	$k_s = 2.51\times10^4$ erg cm^{-1} K^{-1} s^{-1}	Ref. 28
specific heat	$c_{ps} = 1.15\times10^7$ erg g^{-1} K^{-1}	Ref. 28
thermal diffusivity	$\alpha_s = k_s/(c_{ps}\rho_s) = 1.65\times10^{-3}$ cm^2 s^{-1}	
sound velocity [measured by Brillouin spectroscopy (Ref. 29), 40 °C]		
longitudinal wave	$c_{ls} \simeq 3.2\times10^5$ cm s^{-1}	
transverse wave	$c_{ts} \simeq 6.8\times10^4$ cm s^{-1}	
compression modulus	$E = c_{ls}^2\rho_s \simeq 1.3\times10^{11}$ erg cm^{-3}	
shear modulus	$\mu = c_{ts}^2\rho_s \simeq 6.0\times10^9$ erg cm^{-3}	
melting temperature	$T_m = 41.8$ °C	Ref. 30
	$T_m = 41.6$ °C	Ref. 31
heat of fusion	$L = 9.08\times10^8$ erg g^{-1}	Ref. 31
solid-liquid surface tension	$\sigma_{sl} = \epsilon L (M\rho_s^2/N)^{1/3} \approx 20$ erg cm^{-2}	Ref. 32
	$\epsilon \simeq 0.3$	
	M, molar weight $= 214.22$ g mol^{-1}	
	N, Avogadro number	
Liquid		
density	$\rho_l = 1.181$ g cm^{-3} (42.5 °C)	Ref. 33
thermal conductivity	$k_l = 1.80\times10^4$ erg cm^{-1} K^{-1} s^{-1}	Ref. 28
specific heat	$c_{pl} = 1.58\times10^7$ erg g^{-1} K^{-1} (40 °C)	Ref. 28
thermal diffusivity	$\alpha_l = 9.65\times10^{-4}$ cm^2 s^{-1}	
shear viscosity	$\eta_s = 8.4\times10^{-2}$ g cm^{-1} s^{-1}	Ref. 28
constant of self-diffusion	$D_l = \dfrac{k_B T}{6\pi\eta_s a/2} \simeq 8.2\times10^{-7}$ cm^2 s^{-1} [a]	
	$a = \left[\dfrac{M}{\rho_l N}\right]^{1/3} = 6.7\times10^{-8}$ cm	

[a] In Ref. 34 one finds $D_l = 7.5\times10^{-6}$ cm^2 s^{-1} but it is not specified how this value is obtained.

Solving Eq. (A5) numerically for $(t_{n+1}-t_n)$ we find

$$t_{n+1}-t_n \simeq 2.15\frac{l_{\text{crit}}}{v_s} . \tag{A6}$$

For the time lag $\Delta t = t_{n+4}-t_n$, one then obtains

$$\Delta t \simeq 4\times2.15\frac{l_{\text{crit}}}{v_s} = 8.6\frac{l_{\text{crit}}}{v_s} . \tag{A7}$$

Next we calculate the length $l_n(t)$ of the nth step now assumed to be far from the center of the spiral

$$l_n(t) = \int [v_{n-1}(t')+v_{n+1}(t')]dt' , \tag{A8}$$

v_{n-1} and v_{n+1} are the propagation velocities of the adjacent steps. According to Fig. 16 one can put

$$v_{n-1}(t)+v_{n+1}(t) \simeq 2v_n(t) . \tag{A9}$$

Inserting for $v_n(t)$ the expression (A1) one has

$$l_n(t) \simeq 2v_s \int \left[1-\frac{l_{\text{crit}}}{l_n(t')}\right]dt' . \tag{A10}$$

For steps far from the center of the spiral the integral equation (A10) can be solved approximately by replacing $l_n(t')$ in the integral by the asymptotic solution for $t'\to\infty$, namely $l_n(t') = \text{const}+2v_s t'$. One obtains

$$l_n(t) \simeq 2v_s(t-t_0) - l_{\text{crit}}\ln\left[\frac{t}{t_0}\right] , \tag{A11}$$

where t_0 is an integration constant. The spacing d_n between the nth and the $(n+4)$th step is approximately given by (see Fig. 16)

$$d_n(t) \simeq \tfrac{1}{2}[d_{n-1}(t)+d_{n+1}(t)] = \tfrac{1}{2}[l_n(t)-l_{n+4}(t)] . \tag{A12}$$

Since in the steady state of the growth of the spiral

$$l_{n+4}(t) = l_n(t-\Delta t) \tag{A13}$$

one obtains

$$d_n(t) \simeq v_s\Delta t - \frac{l_{\text{crit}}}{2}\ln\left[\frac{t}{t-\Delta t}\right] . \tag{A14}$$

Inserting for Δt the expression (A7) and taking the limit $t\to\infty$ one finds

$$d \simeq 8.6 l_{\text{crit}} . \tag{A15}$$

APPENDIX B: PROPERTIES OF SALOL

Some physical constants of solid and liquid salol are given in Table II.

[1]J. S. Langer, Rev. Mod. Phys. **52**, 1 (1980).
[2]H. A. Wilson, Philos. Mag. **50**, 238 (1900).
[3]J. Frenkel, Phys. Z. Sowjetunion **1**, 498 (1932).
[4]R. Becker and W. Döring, Ann. Phys. (Leipzig) **24**, 719 (1935).
[5]W. K. Burton, N. Cabrera, and F. C. Frank, Philos. Trans. R. Soc. London Ser. A **243**, 299 (1951).
[6]U. Landman, C. L. Cleveland, C. S. Brown, and R. N. Barnett, in *Nonlinear Phenomena at Phase Transitions and Instabilities,* edited by T. Riste (Plenum, New York, 1982), p. 379.
[7]H. Güttinger, J. H. Bilgram, and W. Känzig, J. Phys. Chem. Solids **40**, 55 (1979).
[8]P. Böni, J. H. Bilgram, and W. Känzig, Phys. Rev. A **28**, 2953 (1983).
[9]U. Dürig and J. H. Bilgram, in *Nonlinear Phenomena at Phase Transitions and Instabilities,* edited by T. Riste (Plenum, New York, 1982), p. 371; Helv. Phys. Acta **57**, 241 (1984).
[10]O. N. Mesquita, D. G. Neal, M. Copic, and H. Z. Cummins, Phys. Rev. B **29**, 2846 (1984).
[11]J. H. Bilgram, U. Dürig, M. Wächter, and P. Seiler, J. Crystal Growth **57**, 1 (1982).
[12]H. R. Haller, J. Phys. E **14**, 1137 (1981).
[13]H. Güttinger, M. Gautschi, and E. Serallach, J. Phys. E **9**, 9 (1976).
[14]B. J. Berne and R. Pecora, *Dynamic Light Scattering* (Wiley, New York, 1976), p. 83.
[15]B. J. Berne and R. Pecora, *Dynamic Light Scattering* (Wiley, New York, 1976), Chap. 10.
[16]J. H. Bilgram, in *Cohesive Properties of Semiconductors Under Laser Irradiation,* edited by L. D. Laude (Martinus Nijhoff, The Hague, 1983), p. 237.
[17]K. Kawasaki, Phys. Lett. **30A**, 325 (1969); Ann. Phys. (N.Y.) **61**, 1 (1970); Phys. Rev. A **1**, 1750 (1970).
[18]S. M. Lo and K. Kawasaki, Phys. Rev. A **8**, 2176 (1973).
[19]S. Amelinckx, Naturwissenschaftern **39**, 547 (1952).
[20]H. Bethge, in *Molecular Processes on Solid Surfaces,* edited by E. Drauglis, R. D. Getz, and R. I. Jaffec (McGraw-Hill, New York, 1969), p. 569.
[21]K. Tsukamoto, J. Crystal Growth **61**, 199 (1983).
[22]F. C. Frank, Discuss. Faraday Soc. **5**, 48 (1949).
[23]J. P. Van der Eerden, J. Crystal Growth **56**, 174 (1982).
[24]W. B. Hillig and D. Turnbull, J. Chem. Phys. **24**, 914 (1956).
[25]J. C. Brice, in *Selected Topics in Solid State Physics, Vol. XII,* edited by E. P. Wohlfarth (North-Holland, Amsterdam, 1973).
[26]N. Cabrera and M. M. Levine, Philos. Mag. **1**, 450 (1956).
[27]D. Conti, diploma thesis, Zürich (1978).
[28]K. Neumann and D. M. Al Yawir, J. Crystal Growth **11**, 323 (1971).
[29]H. Z. Cummins (private communication).
[30]K. Neumann, J. Crystal Growth **11**, 313 (1971).
[31]H. Pollatschek. Z. Phys. Chem. A **142**, 289 (1929).
[32]J. H. Hollomon and D. Turnbull, in *Progress in Metal Physics, Vol. IV,* edited by B. Chalmers (Pergamon, London, 1953), p. 357.
[33]G. D. Enright and B. P. Stoicheff, J. Chem. Phys. **64**, 3658 (1976).
[34]S. N. Omenyi, R. P. Smith, and A. W. Neumann, J. Colloid Interface Sci. **75**, 117 (1980).